Axial birefringence induced focus splitting in lithium niobate

Guangyong Zhou,[1] Alexander Jesacher,[2] Martin Booth,[2*] Tony Wilson,[2] Airán Ródenas,[3] Daniel Jaque,[3] and Min Gu[1]**

[1]*Centre for Micro-Photonics and CUDOS, Faculty of Engineering and Industrial Sciences, Swinburne University of Technology, PO Box 218, Hawthorn, Victoria 3122, Australia*
[2]*Department of Engineering Science, University of Oxford, Parks Road, Oxford, OX1 3PJ, United Kingdom*
[3]*GIEL, Departmamento de Fisica de Materiales C-IV, Facultad de Ciencias, Universidad Autonoma de Madrid, Cantoblanco, Madrid, 28049, Spain*
** martin.booth@eng.ox.ac.uk*
*** mgu@swin.edu.au*

Abstract: We report on the experimental observation of "focus splitting" when light is tightly focused into a uniaxial lithium niobate crystal along its optical axis. This effect consists in the focal spot being split into two major sub-peaks along the axial direction. For the microfabrication applications such as three-dimensional photonic crystal fabrication and waveguide writing, this effect is highly undesired since it can lead to the generation of multiple distinct voxels in the vicinity of the focus. The splitting is caused by different birefringence induced aberrations for the ordinary and extraordinary polarization eigenmodes. We present numerical simulations which support our observations and suggest methods to avoid this effect.

OCIS codes: (20.4610) Optical fabrication; (180.0180) Microscopy; (260.1440) Birefringence; (260.1180) Crystal optics.

References and links

1. L. Arizmendi, "Photonic applications of lithium niobate crystals," Phys. Status Solidi **201**(2), 253–283 (2004) (a).
2. R. Osellame, M. Lobino, N. Chiodo, M. Marangoni, G. Cerullo, R. Ramponi, H. T. Bookey, R. R. Thomson, N. D. Psaila, and A. K. Kar, "Femtosecond laser writing of waveguides in periodically poled lithium niobate preserving the nonlinear coefficient," Appl. Phys. Lett. **90**(24), 241107 (2007).
3. J. Thomas, M. Heinrich, J. Burghoff, S. Nolte, A. Ancona, and A. Tünnermann, "Femtosecond laser-written quasi-phase-matched waveguides in lithium niobate," Appl. Phys. Lett. **91**(15), 151108 (2007).
4. L. Gui, H. Hu, M. Garcia-Granda, and W. Sohler, "Local periodic poling of ridges and ridge waveguides on X- and Y-Cut $LiNbO_3$ and its application for second harmonic generation," Opt. Express **17**(5), 3923–3928 (2009).
5. J. Wang, J. Sun, X. Zhang, D. Huang, and M. M. Fejer, "Optical phase erasure and its application to format conversion through cascaded second-order processes in periodically poled lithium niobate," Opt. Lett. **33**(16), 1804–1806 (2008).
6. H. Ishizuki, and T. Taira, "High-energy quasi-phase-matched optical parametric oscillation in a periodically poled $MgO:LiNbO_3$ device with a 5 mm x 5 mm aperture," Opt. Lett. **30**(21), 2918–2920 (2005).
7. J. Kiessling, R. Sowade, I. Breunig, K. Buse, and V. Dierolf, "Cascaded optical parametric oscillations generating tunable terahertz waves in periodically poled lithium niobate crystals," Opt. Express **17**(1), 87–91 (2009).
8. M. Roussey, M.-P. Bernal, N. Courjal, D. Van Labeke, F. I. Baida, and R. Salut, "Electro-optic effect exaltation on lithium niobate photonic crystals due to slow photons," Appl. Phys. Lett. **89**(24), 241110 (2006).
9. G. Zhou, and M. Gu, "Anisotropic properties of ultrafast laser-driven microexplosions in lithium niobate crystal," Appl. Phys. Lett. **87**(24), 241107 (2005).
10. A. Ródenas, G. Zhou, D. Jaque, and M. Gu, "Rare-Earth Spontaneous Emission Control in Three-Dimensional Lithium Niobate Photonic Crystals," Adv. Mater. **21**, 1–5 (2009).
11. R. R. Thomson, S. Campbell, I. J. Blewett, A. K. Kar, and D. T. Reid, "a_ and D. T. Reid, "Optical waveguide fabrication in z-cut lithium niobate ($LiNbO_3$) using femtosecond pulses in the low repetition rate regime," Appl. Phys. Lett. **88**(11), 111109 (2006).
12. G. Zhou, and M. Gu, "Direct optical fabrication of three-dimensional photonic crystals in a high refractive index $LiNbO_3$ crystal," Opt. Lett. **31**(18), 2783–2785 (2006).
13. M. J. Booth, M. A. A. Neil, and T. Wilson, "Aberration correction for confocal imaging in refractive index mismatched media," J. Microsc. **192**(2), 90–98 (1998).

#115734 - $15.00 USD Received 14 Aug 2009; revised 17 Sep 2009; accepted 18 Sep 2009; published 22 Sep 2009

14. M. Booth, M. Schwertner, T. Wilson, M. Nakano, Y. Kawata, M. Nakabayashi, and S. Miyata, "Predictive aberration correction for multilayer optical data storage," Appl. Phys. Lett. **88**(3), 031109 (2006).
15. P. Török, P. Varga, and G. Németh, "Analytical solution of the diffraction integrals and interpretation of wave-front distortion when light is focused through a planar interface between materials of mismatched refractive indices," J. Opt. Soc. Am. A **12**(12), 2660–2671 (1995).
16. M. Gu, *Advanced Optical Imaging Theory* (Springer, 2000).
17. S. Stallinga, "Light distribution close to focus in biaxially birefringent media," J. Opt. Soc. Am. A **21**(9), 1785–1798 (2004).

1. Introduction

Lithium niobate ($LiNbO_3$) is an extremely versatile ferroelectric nonlinear crystal material that has been widely used for integrated photonic applications [1–3] such as fast switches, interconnects, electro-optically-controlled multiplexers and demultiplexers, and nonlinear optical waveguides. In addition, rare-earth ions can also be incorporated to activate $LiNbO_3$ for exploiting the radiation controlling of emitter by photonic crystals, opening the way to unique functional integrated laser systems. Its nonlinearity makes it interesting for various optical applications such as second harmonic generation [4,5], optical parametric oscillation [6,7] and electro-optical modulation [8]. Due to its rather high refractive index and high nonlinearity, it is also an excellent material for 3D nonlinear photonic crystal fabrication. By tightly focusing a femtosecond (fs) laser beam into the crystal, the nonlinear absorption can generate sub-micron sized regions of modified refractive index, or even an amorphous region (referred to hereafter as a "voxel") if the power is sufficiently high [9–11]. However, the refractive index mismatch between the objective immersion oil and $LiNbO_3$ introduces strong spherical aberration to the incoming beam, the magnitude of which is proportional to the focusing depth [12]. The spherical aberration reduces the peak intensity at the focus and therefore limits the fabrication depth in the manufacturing process of 3D microstructures. In isotropic materials, the aberration caused by a refractive index mismatch has been investigated intensively [13–15] and can be compensated for by "pre-aberrating" the beam with a conjugate phase aberration using an adaptive optical element [13]. In the case of uniaxial $LiNbO_3$ however, the situation is more complex. Due to its birefringence, the refractive index for the extraordinary component of an incident beam depends on its propagation direction. This gives rise to additional phase aberrations, since the individual rays of a tightly focused laser beam have different propagation directions: the originally spherical wavefront gets distorted due to the different optical path lengths of the individual rays of the cone. Although the birefringence of $LiNbO_3$ is relatively weak (n_o-n_e = 0.07934) compared to the refractive index mismatch between the crystal and the immersion oil (Δn = 0.7), this additional aberration can have a strong effect on the fabrication process. In previous work [9], these anisotropic properties were observed when direct-laser-writing (DLW) was performed along different directions in $LiNbO_3$, and it was found that the fabrication is problematic when the beam is focused parallel to the optical axis of the crystal. In this case the focus quality degrades more rapidly while increasing the focusing depth and we observed for the first time, to the best of our knowledge, a novel "focus splitting" phenomenon but could not give detailed explanation on the mechanism of the splitting effect.

In this paper we systematically investigate how the birefringence affects the DLW process when a high numerical aperture (NA) objective is used. Our investigations include the direct femtosecond laser fabrication of voxels along different crystal orientations together with numerical simulations.

2. Experiments

The crystal used in our experiments was a co-doped MgO:Er^{3+}:Yb^{3+}:$LiNbO_3$. The MgO dopant is used to increase the damage threshold of $LiNbO_3$ and rare earth ions (Er^{3+}, Yb^{3+}) are used to optically activate the crystal for further fluorescence investigations (which are however out of the scope of this paper). The dopants have only little influence on other properties such as refractive index and birefringence. The crystal was cut into small pieces with dimensions of 1.5mm × 1.5mm × 10 mm, the four larger surfaces of which were polished

#115734 - $15.00 USD Received 14 Aug 2009; revised 17 Sep 2009; accepted 18 Sep 2009; published 22 Sep 2009

to optical quality. The laser beam came from a regenerative amplifier (Spitfire Pro, Spectra-Physics) which emits 120 fs pulses of linearly polarized light at 800 nm with a pulse repetition rate of 1 kHz. The absorption of Er^{3+} and Yb^{3+} rare-earth ions at the laser wavelength was observed not to affect the DLW process. The linearly polarized laser beam was tightly focused into $LiNbO_3$ by using an oil immersion objective (NA1.45). In the fabrication process, 50 pulses (50 ms exposure time) were used to generate the voxels. Voxels were fabricated at different depths and close to the edge of the crystal (~20 μm), allowing us to image the side view of the voxel after fabrication by turning the sample by 90 degrees. In order to get clear voxels, we increase the power from 50 mW for a depth of 5 μm to 220 mW for a depth of 50 μm. The experimental setup was the same as that described elsewhere [8] except that an infrared-enhanced Olympus (100 × , NA1.45, oil) objective. The voxels were characterized by using a laser scanning confocal microscope (Fluoview, Olympus, Japan).

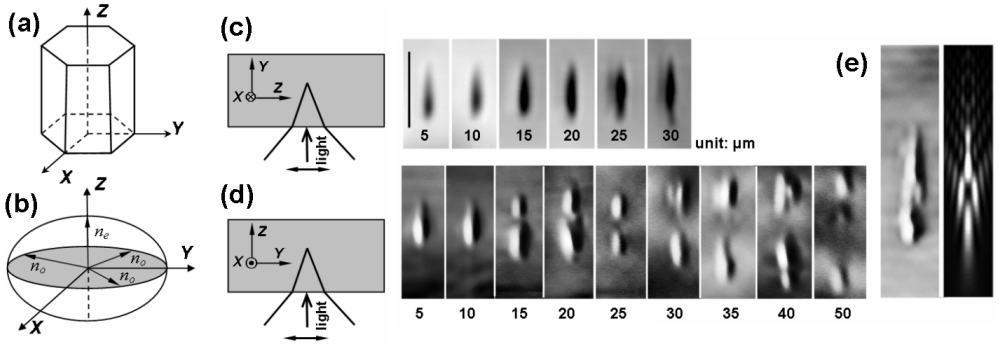

Fig. 1. (a) Sketch of the crystalline directions; (b) Sketch of index ellipsoid of $LiNbO_3$; (c) and (d) Confocal transmission microscopy images of voxels in $LiNbO_3$, which resemble the corresponding intensity distributions in the focal region. (c) Writing along the Y-crystal direction, focus depths: 5 μm to 30 μm, scale bar: 5 μm ("↔" polarization). (d) Writing along the Z-crystal direction, focus depths: 5 μm to 50 μm ("↔" polarization). (e) Comparison between experimental (left) and numerical simulation (right) at 30 μm depth and Z-direction.

Figure 1 shows the side view of several voxels, which were generated in different depths and with different crystal orientations. Figure 1a shows the crystal directions where Z direction is along the optic axis. Figure 1b shows the sketch of the index ellipsoid of $LiNbO_3$ where $n_o > n_e$. During the inscription process, the sample is stationary without moving in any direction. The focusing directions were chosen to be transverse and parallel to the optic axis of the crystal, called Y- and Z-crystal direction, respectively. In the images, the light is focused up from the bottom. The voxels created by focusing along the Y-direction (Fig. 1c) show a clear axial elongation, which gets more pronounced at larger fabrication depths. This indicates a dominance of spherical aberration. When the light is focused along the Z-direction (Fig. 1d) however, up to three distinct voxels are created along the focusing axis, which are henceforth referred to as the first, second and third voxels, with the first voxel close to the objective. We observed this "focus-splitting" to occur at fabrication depths larger than 15 μm. At even larger depths we could also observe the generation of additional off-axis voxels, which are most likely created by side lobes of a strongly aberrated focal spot (see the right image of Fig. 1e).

3. Theoretical simulation and discussions

The reason for the observed focus splitting phenomenon is the birefringence of $LiNbO_3$. Based upon vectorial Debye theory [16], Stallinga has modeled light focusing into weakly birefringent materials [17]. Our following considerations develop this work and apply it to high numerical aperture focusing into the high refractive index, birefringent $LiNbO_3$. For simplicity, we only cite the key concepts of that paper and exclude the complex equations.

According to the relative orientation of the optical axis to the focusing direction, one can derive two polarization eigenmodes, the polarization states of which remain unchanged during

#115734 - $15.00 USD Received 14 Aug 2009; revised 17 Sep 2009; accepted 18 Sep 2009; published 22 Sep 2009

propagation through the crystal. These correspond to the extraordinary (*e*-mode) and ordinary mode (*o*-mode). It is further possible to derive the individual aberration functions for these eigenmodes [17]. Since the refractive index of the *o*-mode is independent of the propagation direction, its phase aberration corresponds to that of a "classical" refractive index mismatch, i.e. it is purely spherical. The aberration function of the *e*-mode however is more complex and can also be non-rotationally symmetric. The polarization eigenmodes for the Y- and Z-direction cases are shown in Fig. 2, together with the corresponding phase aberration functions. These cases were derived using the formulation described in Ref [17]. For clarity of illustration, the dominant mean refractive index induced spherical aberration and defocus has been removed (using the average refractive index of 2.2291). The analysis shows that the eigenmodes of the Z-direction case are radially and azimuthally polarized. The corresponding aberration functions show a significant difference in defocus, which explains the observed focus splitting: The linearly polarized beam is decomposed into the *e*- and *o*-mode components with equal energy, but with asymmetric field distributions. For the *e*-mode, the intensity is distributed along the linear polarization direction whereas for the *o*-mode, the intensity is distributed orthogonally. The difference in defocus means that the light of each mode is focused at a different axial position. On the other hand, the eigenmodes of the Y-direction are almost perfectly linearly polarized, with only slight deviations near the edges of the pupil. The *e*-mode suffers mainly from astigmatism and the *o*-mode from an additional small amount of spherical aberration, which is caused by the difference between n_o and the average refractive index. Linearly polarized illumination can be aligned so that only one of these eigenmodes is effectively excited. Even if both modes are produced, since there is no significant difference in defocus between two functions, no splitting of the focus occurs.

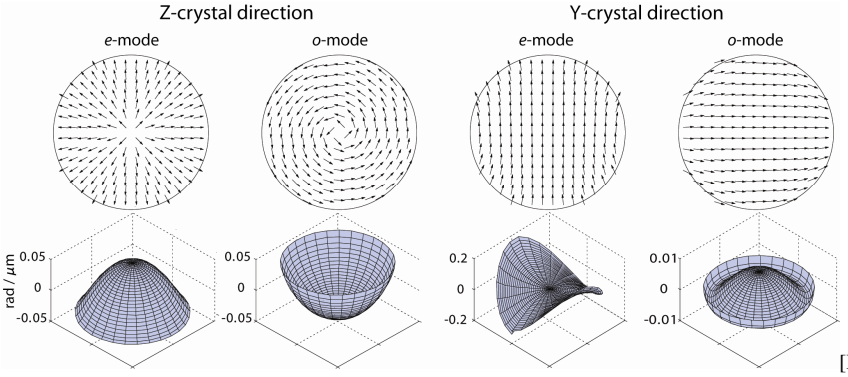

[REMOVED SHAPE FIELD]

Fig. 2. Polarization eigenmodes for focusing along Z- and Y-crystal direction (top row). The vector diagrams show the polarization profiles of transverse cross-sections through collimated beams. The corresponding phase aberration functions per micron focusing depth are shown below. Both polarization profiles and phase aberrations were calculated for our system parameters.

We performed numerical simulations of focal intensity distributions using the method described in Ref [17]. We treated the cases of focusing into isotropic media as well as focusing into $LiNbO_3$ along the Y- and Z-crystal directions. The refractive index of the isotropic medium was assumed to be 2.2291, which is the average of n_e and n_o of $LiNbO_3$ at the wavelength of 800 nm. Linear polarization along the Y-direction was used. We performed detailed simulations for the interesting case of focusing along the optical axis of $LiNbO_3$, where the focus splitting occurs. We calculated the axial focal intensity distributions for different fabrication depths. The results for 15 µm, 30 µm and 45 µm are shown in Fig. 3a. The simulations clearly show several distinct sub peaks for focusing depths larger than 15 µm. For depths less than 15 µm, the main peak is dominant and there is no second peak. As the light is focused deeper, there appears a clear second peak (with several sub-peaks) which is as strong as the first one at 30 µm. At even larger focal depths, the second peak is even stronger

#115734 - $15.00 USD Received 14 Aug 2009; revised 17 Sep 2009; accepted 18 Sep 2009; published 22 Sep 2009

than the first peak. On the other hand, when the light is focused along the Y-crystal direction, there is no focus splitting. For comparison, Fig. 3b shows the corresponding intensity plots for the Z- and Y-direction cases in $LiNbO_3$ as well as for an "assumed" isotropic crystal with the mean refractive index of $LiNbO_3$. The nominal focusing depth was taken to be 30 µm. The peak intensity is maximal for the isotropic case.

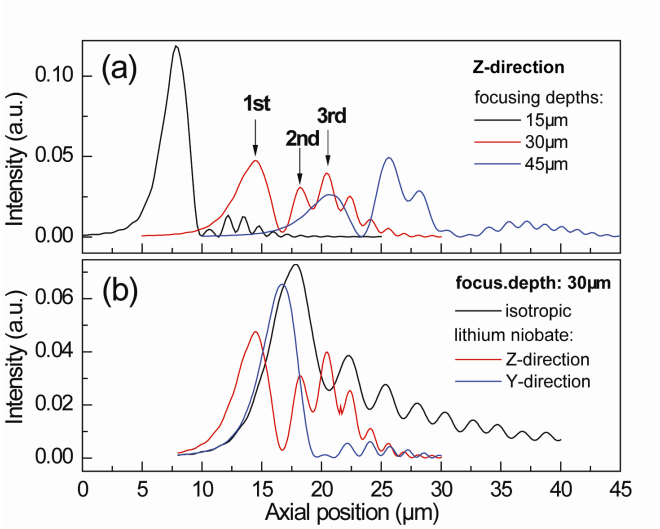

Fig. 3. (a) Calculated axial focal intensity distributions when linearly polarized light is focused 15 µm, 30 µm and 45 µm deep into $LiNbO_3$ along the Z-direction. The axial position is measured relative to the position of the focus without presence of the crystal, i.e. it reflects the focal shift caused by the refractive index mismatch between crystal and immersion oil. (b) Calculated axial focal intensity distributions when linearly polarized light is focused 30 µm deep into $LiNbO_3$ along the Z- and Y-directions as well as into an isotropic medium with a refractive index of 2.2291.

When the laser beam is focused along the Y-direction, the side lobes to the right are much less pronounced and the full width at the half maximum (FWHM) is smaller (3.3 µm compared to 4.4 µm). However, the total on-axis intensity in the Y-direction case is also much smaller (48% of the isotropic case), which indicates that more light is distributed in off-axis areas. When light is focused along the Z-direction, the discussed focus splitting becomes apparent: the on-axis intensity shows two major peaks with the second one being divided into several sub-peaks. Due to this focus splitting effect, the global peak intensity is much smaller than in the Y-direction case.

In order to compare the simulation with experimental observation, the relative positions of the simulated on-axis intensity maxima and the observed on-axis voxels have been recorded in Fig. 4. The voxel distances were measured from contrast enhanced confocal images similar to those in Fig. 1(b). For each focusing depth at least three images of different fabricated voxels have been evaluated. Hence, the error bars in Fig. 4 reflect the uncertainty of the distance measurements taken from the images as well as possible real variations in the voxel positions. The position of the first voxel acts as reference and is therefore always 0 µm. From Fig. 4 we can clearly see that the distances of the 2nd and the 3rd voxel to 1st voxel increase with the fabrication depth, whereas the spacing between the 2nd and the 3rd voxel is approximately constant. These observations hold for both the simulation and the experimental data. Also the spacing between the 2nd and 3rd voxels is correctly predicted. These results suggest that the origin of the focus splitting is indeed from the birefringence.

The measured spacing between the voxels is smaller than that predicted by the theory. Another discrepancy occurs in the relative size of the voxels. In Fig. 4, filled/hollow markers indicate whether the 2nd or 3rd voxel is more/less pronounced. According to our simulations, the 3rd peak should be dominant for fabrication depths up to 30 µm, whereas the 2nd voxel

#115734 - $15.00 USD Received 14 Aug 2009; revised 17 Sep 2009; accepted 18 Sep 2009; published 22 Sep 2009

should become more pronounced at larger depths. Interestingly, we observe the contrary behaviour: the second hole is dominant for depths up to 30 µm, whereas no formation of a third voxel could be observed at 15 µm and 20 µm depth, even at moderate power levels. The observed discrepancies could possibly be explained by initial system aberrations. Initial spherical aberration for instance, which is not uncommon in microscope set-ups, could possibly contribute to the parallel shift between the theoretical and experimental data sets. Similarly, initial aberrations could also account for the observed mismatch in the prominence of the individual sub-peaks.

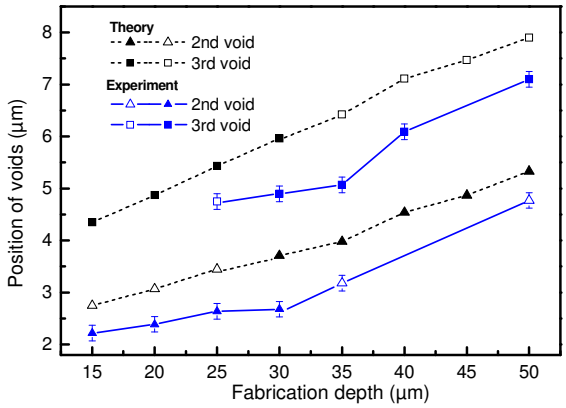

Fig. 4. Experimental and theoretical results of birefringence-induced focus splitting. The light beam is focussed along the Z-direction. Dashed black lines: Expected positions of the second and third voxels with respect to the first one. Thick blue lines: Observed positions of the generated the second and third voxels with respect to the first voxel. Filled markers indicate whether the second or third peak is dominant. The lines serve as a guide for the eye.

4. Conclusions

The birefringence induced focus splitting phenomenon has been investigated both theoretically and experimentally. When the laser beam is focused along the optic axis of the crystal, the focus splitting phenomenon starts to appear at a focusing depth of roughly 15 µm and voxel separation of up to 7 µm has been observed at larger depths. The effect is also predicted by a vectorial Debye theory based approach which attributes the focus splitting to the existence of two significantly different aberration functions for the two polarization eigenmodes.

The results suggest that in order to fabricate high quality microstructures in anisotropic crystals, the polarization of the laser should match that of one polarization eigenmode. Ideally one can use the crystal in the Y-direction, since then linearly polarized light in the X- and Y-directions already closely matches the polarization eigenmodes. If however the fabrication direction must correspond to the optic axis of the crystal, one could use radially or azimuthally polarized light to remove the focus splitting, although this will affect the intensity distribution of the focus.

Acknowledgments

This work was supported by the Australian Research Council (ARC) Centre of Excellence for Ultrahigh-bandwidth Devices for Optical Systems (CUDOS, No. CE0348259), an ARC Discovery grant (No. DP0665868), the Austrian Science Fund (J2826-N20), the Leverhulme Trust (UK), and the Spanish Ministerio de Educación y Ciencia (MAT2004-0334 and MAT2007-64686).

#115734 - $15.00 USD Received 14 Aug 2009; revised 17 Sep 2009; accepted 18 Sep 2009; published 22 Sep 2009